Analyst

Accepted Manuscript

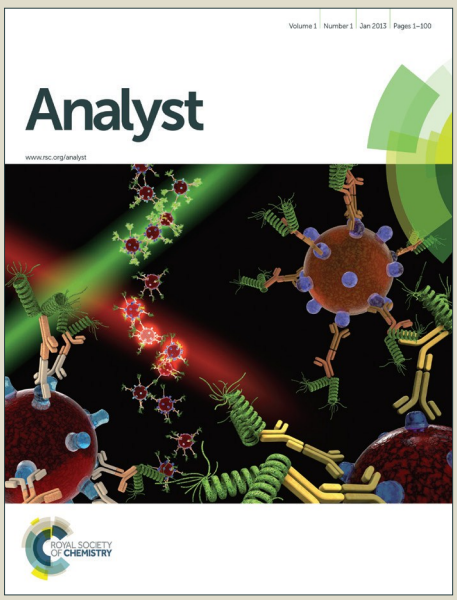

ROYAL SOCIETY OF CHEMISTRY

www.rsc.org/analyst

Concentration of Sindbis Virus with Optimized Gradient Insulator-based Dielectrophoresis

Jie Ding,[a] Robert Lawrence,[c,d] Paul V. Jones,[a] Brenda G. Hogue,[b,c,d] and Mark A. Hayes[*a]

[a]School of Molecular Sciences, Arizona State University, Tempe, Arizona

[b]School of Life Sciences, Arizona State University, Tempe, Arizona

[c]The Center for Infectious Diseases and Vaccinology; [d]Center for Applied Structural Design, The Biodesign Institute, Arizona State University, Tempe, Arizona

Corresponding Author:

Dr. Mark A. Hayes
Arizona State University
School of Molecular Sciences
Mail Stop 1604
Tempe AZ 85287
mhayes@asu.edu
Ph. (480) 965-2566, FAX (480) 965-2747

Abbreviations: dielectrophoresis (DEP), point of care diagnostic devices (POC), Tobacco Mosaic (TMV), Herpes simplex (HSV), gradient insulator-based dielectrophoresis (g-iDEP), Sindbis virus (SINV), heat resistant strain of Sindbis virus (SVHR), dynamic light scattering (DLS), transmission electron microscopy (TEM)

Keywords: Sindbis virus, dielectrophoresis, concentration, isolation, detection, electrophoresis, submicron bioparticles, electrokinetics

Total Words (excluding title page):

Abstract

Biotechnology, separation science, and clinical research are impacted by microfluidic devices. Separation and manipulation bioparticles such as DNA, protein and viruses are performed on these platforms. Microfluidic systems provide many attractive features, including small sample size, rapid detection, high sensitivity and short processing time. Dielectrophoresis (DEP) and electrophoresis are especially well suited to microscale bioparticle control and have been demonstrated in many formats. In this work, an optimized gradient insulator-based DEP device was utilized for concentration of Sindbis virus, an animal virus with a diameter of 68 nm. Within only a few seconds, the concentration of Sindbis virus can be increased by two to six times in the channel under easily accessible voltages as low as about 70 V. Compared with traditional diagnostic methods used in virology, DEP-based microfluidics can enable faster isolation, detection and concentration of viruses in a single step within a short time.

Introduction

Detection, isolation, and identification of viruses are key steps in the diagnosis of the infectious diseases and are prerequisites for research that leads to vaccines, treatments, and therapies.[1-4]

The initial indicator of a viral infection is generally made by observation of symptoms by the host. Establishing the virological cause can require a lengthy diagnostic process, particularly if the causative virus is rare. The early detection methods relied on demonstration of infection in a susceptible host, including animals, embryonated eggs, organ cultures or plants.[5,6] Among various biological and physical approaches, plaque assay is the most elegant, quantitative and useful. It was developed in the early 1900s for the study of bacteriophage.[7] However, the measured presence of infectivity doesn't necessarily correspond to the number of virus particles in a preparation and some viruses require cells in distinct states.[5] In response, focus assay based on transformation cytopathology[8,9] and the endpoint-dilution assay based on detectable pathology[10] were developed. These methods still have long analysis times (up to 4 weeks), relatively poor sensitivity and are susceptible to bacterial contamination.

Serological methods based on antibody-antigen recognition are a mainstay of viral diagnosis today and include immunofluorescence techniques[11-13], enzyme linked immunosorbent assay[14-16], western blot[17-19], green fluorescent protein[20], and a host of other less common approaches. Nucleic acid-based assays that rely on polymerase chain reaction (PCR) methods are commonly used both for identification and quantification of viruses.[21] DNA microarrays and high-throughput sequencing methods can positively identify an unknown viral pathogen.[22] For many of these techniques, the sensitivity and specificity depend greatly on the choice of antigen or target sequence and detection reagents, including antibodies and specific nucleic acid probes.

Direct assays include electron microscopy (EM) methods to observe the morphology of viruses or EM immuno-based detection of viruses.[23] However, considering that most viruses share similar rod or icosahedral morphologies, common transmission electron microscopy (TEM) is not sensitive enough to produce the high-resolution images needed for identification. Cyro-EM is capable of producing the near atomic-level resolution of virus constructions without chemically altering original viral structures.[24,25] However, this technique is limited by the requisite concentrated sample[5] and the extensive amount of time and resources that are required to produce high resolution images. It is not feasible to discern all viruses from morphological data alone even when high quality images are obtained.

Isolation and purification of a virus from its host require another set of techniques including column chromatography, centrifugation, and microfluidics.[26-34] Centrifugation is a classic, powerful, and common technique for separation and purification of bioparticles. But it does have some limitations, including low efficiency for separating particles with similar density, such as proteins and viruses.[26] Separation techniques based

on membrane systems were developed in the last 30 years and are still attracting considerable attention.[27,28] The membrane system is suitable for large-scale processes and the efficiency is highly dependent on the affinity of targets to specific membranes. Also, the pore size of membranes is a sensitive variable that affects efficient separation.

Chromatographic methods, such as size exclusion and ion exchange, are also used to separate and purify viruses based on differences in size and charge characteristics.[29,30] Similar to membrane separation techniques, these are used for large-scale preparations and suffer from low efficiency and selectivity challenges, due to the limited pore size choices.

Separation techniques based on microfluidics show great potential for practical application of virus isolation.[31-34] Microfluidics systems can enable identification, isolation and quantification of a virus in a single technique that allows for small sample size, rapid detection, high sensitivity and short processing time. Recently, quite a few advanced microfluidic techniques, such as dielectrophoresis (DEP)-based microfluidic techniques, have been developed and applied to separation of viruses.

Dielectrophoresis-based virus analysis was first explored in 1996, when Muller et al.[35] examined the trapping and enrichment of viruses in aqueous environment while the corresponding theory and simulation was accomplished by Schenelle et al.[36]. This successful trial extended the size limit of DEP manipulation to the submicron level and provided an initial example of DEP application for virus isolation and detection. For the following decade, more AC-electrode DEP-based microdevices were developed for plant and relatively large animal viruses, including tobacco mosaic virus (TMV)[37-39] and herpes simplex virus (HSV)[39-42]. Unique DEP properties allowed successful separation of TMV and HSV under AC-DEP conditions.[39] To overcome potential disadvantages of AC-DEP, improvements with AC-electroosmotic flow approaches have resulted in higher throughput of the concentrated virus.[43]

DC-insulator-based DEP devices were introduced with their advantages of easier fabrication, more robust operation and a chemically inert environment. It was applied to viruses in 2003, when Lapizco-Encinas and colleagues[44] first observed the trapping and streaming of bacteriophage T4. After that, TMV was also manipulated with the same strategy.[45] A similar DEP technique was recently used to concentrate influenza virus particles to facilitate trapping of a single particle with optical tweezers and subsequent infection of a cell with the isolated virus.[46]

Incorporation of micron-sized channels in microfluidic devices can provide an alternative, perhaps more efficient and power-saving method for virus detection and separation. This approach is explored here using the sawtooth-patterned gradient insulator-based DEP (g-iDEP) device. This technique was first introduced in 2007, featuring a progressive change in the tooth geometry which can create distinct zones of increasing local field gradient along the length of the channel (Fig. 1).[47] The details of the previous design was introduced by Staton et al.[48], where the gap distance decreased

gradually from initial 945 μm to final 27 μm by increasing the side length and width of each PDMS triangles by 40 μm after every 6 repeats. It has demonstrated isolation and concentration of polystyrene particles[48], red blood cells[49], amyloid fibrils[50], *Escherichia coli* serotypes[51], and *Staphylococcus epidermidis* strains[52]. The relatively linear change of the physical size of the gates caused most of the capturing phenomena to be observed in the last two sets of gates and sub-micron particles could not be captured. Based on mathematical expressions for electrokinetic/dielectrophoretic capture[53], the following expression is used to represent conditions for particle trapping at a gate:

$$\frac{\nabla|\boldsymbol{E}|^2\cdot\boldsymbol{E}}{E^2} \geq \frac{\mu_{\mathrm{EK}}}{\mu_{\mathrm{DEP}}} \quad , \qquad \textbf{(1)}$$

where $\boldsymbol{E}$ is the electric field, μ_{EK} and μ_{DEP} are the electrokinetic mobility and dielectrophoretic mobility of the particle, respectively. Importantly, this expression relates electric field parameters within the channel directly to the intrinsic properties of analytes. To simplify the present discussion this field-related term, $\frac{\nabla|\boldsymbol{E}|^2\cdot\boldsymbol{E}}{E^2}$ is expressed as e_c, the concomitant electromotive force experienced by a particle. The value of e_c were too low in these previous designs to capture small particles.

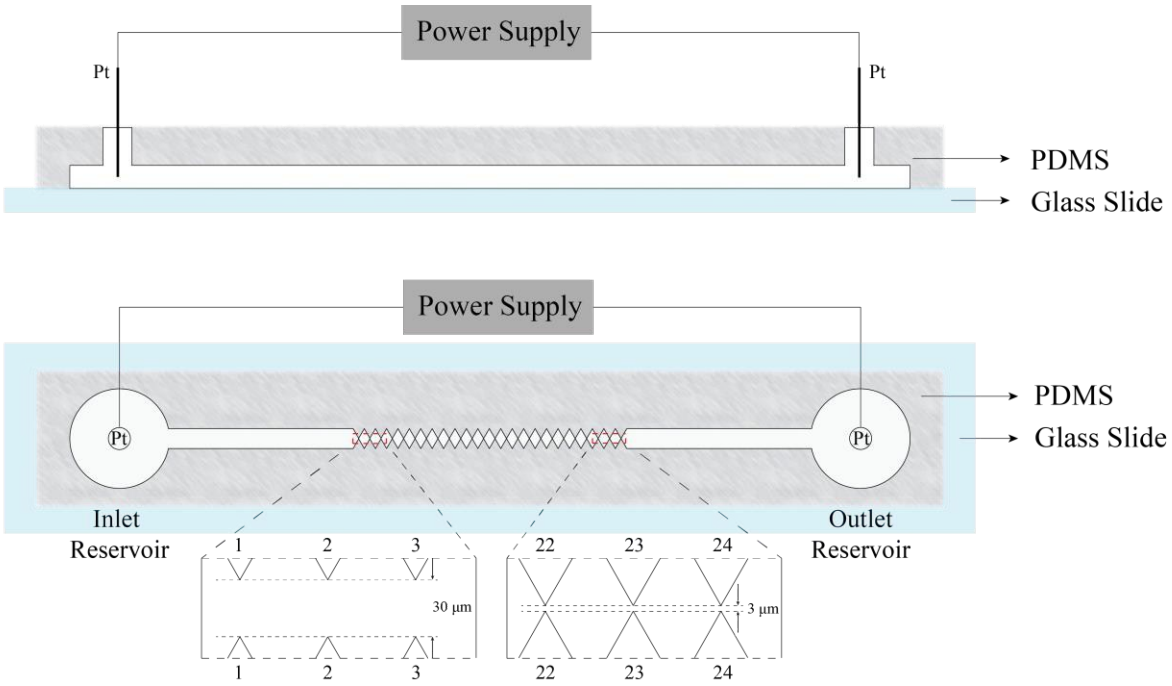

Figure 1. Illustration of the sawtooth gradient insulator-based dielectrophoresis device in side view (Top) and in vertical view (Bottom). Approximately 4 cm long, with a 500-μm wide, 20-μm deep open channel between two reservoirs with electrodes. The channel is constricted to an increasing degree by triangular insulting wall protrusions. These structures induce local increases in electric fields and gradients, providing capturing zones of increasing strength.

Sindbis virus (SINV) was used as the model to test this new channel design. The virus is a member of the *Togaviridae* family that includes a number of medically important viruses that infect humans and other animals. SINV is transmitted by mosquitoes.[54] The virus is an enveloped icosahedrally structured with a ~70 nm diameter.[55] The virus is composed of three major structural components, two glycoproteins (E1 and E2) and a capsid (C) protein.[56] The E1 and E2 proteins form heterodimers that associate as 80 trimers that are anchored in the lipid envelope.[57] Inside the envelope, 240 capsid proteins are assembled as an icosahedron that surrounds the ~11.7 kb positive sense, single-stranded RNA genome. Protein, RNA and lipids make up roughly 64%, 9%, and 27%, respectively of the total mass of SINV particles.[55] The near-spherical structure also makes it a good model for testing in DEP systems, since most theories are based on using the spherical target as default. Considering all these, Sindbis virus is used as a representative virus with a relatively small size and a near-spherical icosahedral structure in this work.

In this paper, we demonstrate that the first time that a heat resistant strain of Sindbis virus (SVHR) is captured using an evolved g-iDEP device. This device was designed and fabricated specifically for capturing submicron bioparticles and demonstrated isolation and concentration of SVHR. Under these specific experimental condition, SVHR behaves as positive dielectrophoresis (*p*-DEP) particle, which is different from most of previous related group work in with other bioparticles, such as bacteria and red blood cells.[49,51,52] The SVHR responded to applied voltage as low as 70 V, easily accessible with most power supplies. Further investigation on the reproducible accumulation phenomenon indicates that the higher applied voltage and longer time period would facilitate increased concentration of SVHR in the capturing zone.

Experimental

Sindbis Virus Preparation and Characterization

A heat resistant strain of Sindbis virus (SVHR) was cultivated as previously described by Hernandez et al.[58] Briefly, baby hamster kidney cells were grown in minimal essential medium supplemented with 5% fetal bovine serum, 5% tryptose phosphate broth, 2 mM L-glutamine, and 50 μg/mL gentamycin. Cells were grown to near confluence before infection with SVHR at a multiplicity of infection of 0.1. Infected cells were further incubated in Glasgow minimal essential medium containing the same supplements as the MEM media, plus an additional 2 g/L of $NaHCO_3$. At 26 h after infection the medium was removed from infected cells and clarified by centrifugation for 10 min at 1000 x g to remove cell debris.

Harvested virus colloid was purified by centrifugation through two gradients prepared from potassium tartrate (dibasic hemihydrate) dissolved in PN buffer (100 mM NaCl, 50 mM PIPES pH 7.2). First, the clarified medium was sedimented on a continuous 15-37% potassium tartrate density gradient. Gradients were fractionated and the appropriated

density fractions containing virus were pooled. The pooled fractions were with PN buffer and overlayed onto a step gradient consisting of 37% potassium tartrate overlayed with 15% potassium tartrate. Virus was collected from the gradient interface by fractionation. Both gradients were centrifuged at 100,000 x g for 4 h at 4 ℃. Following gradient purification, the virus was dialyzed in PN buffer to remove potassium tartrate. The purified virus was inactivated by addition of glutaraldehyde to a final concentration of 0.01% v/v and incubating at 4 ℃ for 24 h. Dialysis was repeated to remove the glutaraldehyde. The concentration of purified virus was determined using a modified Lowry Assay adapted for membrane protein determination.[59] A concentration of 1 mg/mL of SVHR was equated to 3 x 10^{11} plaque forming units (pfu)/mL, based on corresponding plaque assays of non-inactivated SVHR in BHK cells. The methods for titration by plaque assay were carried out according to Hernandez et al.[58]

Labeling Virus with Fluorophore (Rhodamine)

Inactivated SVHR was suspended in PN buffer, mixed with NHS-Rhodamine (Thermo Scientific, Rockford, IL, USA) solution and incubated at 4 ˚C overnight to label the virus. Excess dye was removed by pelleting the virus at 100,000 x g in a SW55Ti rotor (Beckman Coulter Inc., Brea, CA, USA) for two hours. The pellet was washed twice through resuspension and repelleting prior to final resuspension in 10 mM NaCl, 10 mM PIPES pH 7.2. For some experiments, the virus colloid was dialyzed at 4 ˚C using a 3500 MWCO Slide-A-lyzer mini cassette (Thermo Scientific, Rockford, IL, USA). The conductivity of the buffer was measured to be 2.12 mS/cm (Traceable conductivity meter, Fisher Scientific, Hampton, NH, USA) The final estimated concentration of SVHR was 0.375 - 1.5 × 10^{11} pfu/mL, based on the original titer that was determined by plaque assay and losses during preparation.

Characterization of Labeled Virus

Dynamic light scattering (DLS) and TEM were used to determine the size distribution and confirm intact morphology of virus, respectively, before and after labeling. DLS measurements were carried out with a Spectro Size 302 (Molecular Dimensions, UK), equipped with a 785 nm laser. For each measurement, the laser was directed at a 3-5 µL hanging droplet of the sample suspended from a siliconized glass cover slide. Data was compiled from ten separate 20 s measurements. Settings included a shape factor of 1.0, exponent of 3.0, and refractive index of 1.339. Correlation of the resulting signal to the sample was validated by a sigmoidal autocorrelation function. A narrow size distribution is indicative of a monodispersed sample. TEM was carried out with a beam energy of 80 kV. Virus (5 µL) was spotted onto 300-mesh copper grids with formvar support film (Electron Microscopy Sciences) and incubated for 5 min. The grid was blotted dry and negatively stained with 5 µL of 2% uranyl acetate. The grid was again blotted dry prior to imaging.

Device Fabrication

The microfluidic device was fabricated by an established procedure of photolithography, fabrication, and bonding techniques.[48,51,60] The channel configuration was first designed using Adobe Illustrator (Adobe Systems Inc., San Jose, CA) and printed onto a chrome-glass photomask (J D Photo-Tools LTD., Oldham, Lancashire, UK). With the photomask, a silicon wafer was then made using photolithography and dry etching techniques. PDMS casts were made from the silicon wafer using a Sylgard 184 silicone elastomer kit (Dow Corning Corp., Midland, MI, USA). Access holes were created with a 3 mm Harris Uni-Core punch (Shunderson Commnications Inc., Orleans, Ontario, Canada). PDMS casts were washed with isopropanol and water and sonicated for 30 s (Aquasonic ultrasonic cleaner, VWR International, Radnor, PA, USA). Glass slides were washed with acetone, isopropanol, and water successively before being sonicated for 10 s. The PDMS casts and glass slides were dried with N_2 gas and treated with high level O_2 plasma for 60 s (Plasma Cleaner, Harrick Plasma, Ithaca, NY, USA) before contact sealing.

A new design of a g-iDEP device is developed for generating linear gradient for tooth-to-tooth of $\nabla E^2/E$ ratio[61] and for smaller bioparticles targets, such as viruses and proteins (larger magnitude ∇E^2 factors are necessary). Generally, the device has two reservoirs on both ends of the channel into which electrodes are placed and connected to the power supply. The central part of the channel is constructed of 24 sawtooth shaped constrictions, which are similar to those used in previous gradient insulator-based dielectrophoresis devices (referred to as V1)[47,48,50,51], though specific sizes for the constrictions have been adjusted for the new design (V2, Fig. 1) used here. In V1, the dimensions of the channel were designed by changing the size of the insulating-60 degree triangles, which started with 6 μm for base-length and 5.2 μm height. From inlet to outlet, their side length and width were designed to increase by 40 μm after every six repeats, which resulted in the gap distance (closest approach of the teeth tips) varying from 945 μm to 27 μm. Most particle capture occurred at the last 3 sets of gates with V1.[47,48,50,51] For the current studies, it is important to distribute the capturing conditions throughout the channel, especially for smaller particles. To evaluate the design improvement, the value of $\nabla E^2/E$ on the centerline of the channel, which is parallel to the channels long axis and all the midpoints between each pair of sawtooth points are located on, was computed using finite-element multiphysics software. Based on the phenomena of previous experiments with V1, the specific size of constriction between each pair of sawteeth was adjusted, plotted using AutoCAD software and then verified by simulation (next section). The new design was optimized through this procedure until the linear trend line was achieved for the values of $\nabla E^2/E$ on the centreline of the gates. The final dimensions of V2 were set and the distance between the sawtooth tips at each constriction repeats every three with a decreasing trend varying from 30 μm near the inlet reservoir (left) to 3 μm near the outlet reservoir (right).

Finite-Element Model Calculations

Modeling was performed with finite-element multiphysics simulation software (COMSOL Inc., Burlington, MA) to investigate the electric field characteristics in the microchannel. The model consisted of a 2D representation of the main channel at the same scale as the experimental device. The electric potential in the channel is presumed to be relatively consistent across the small depth of the microchannel, therefore a 2D approximation of the channel was used to simplify the simulation.

Using the *electric currents* physics interface under AC/DC module of COMSOL Multiphysics, the boundaries of the imported channel geometry were set as insulators by default. Insulator boundaries were defined as silica glass while the bounded domain was assigned as water using the build-in materials library. The applied potential was assigned as a user-adjustable input variable. The boundary representing the microchannel inlet (on the left side) was designated as ground. The opposing boundary representing the microchannel outlet (on the right side) was assigned at -100 to -3000 V, reflecting a variety of experimental conditions.

The software uses finite-element modeling to solve the boundary value problem for the underlying physics. User-adjustable parameters allow fine-tuning of mesh characteristics, with the goal of minimizing error and noise. For these simulations, a *free triangular* mesh was used with empirical adjustments to the mesh structure. The mesh was optimized for accuracy of modeling within narrow channel segments and regions near gates, while attempting to minimize computation time.

Results were computed using a *stationary* solution. From these results, 2D plots, line charts, and numerical values were obtained using expressions for $\boldsymbol{E}$, $\boldsymbol{\nabla}|\boldsymbol{E}|^2$, and trapping conditions estimated for simple particles similar to the bioparticles in question.

Procedure

The internal channel of the device was rinsed with running buffer (10 mM NaCl and 10 mM PIPES pH = 7.2) and treated with 4 mg/mL BSA to reduce electroosmotic and nonspecific absorption. A 10 μL aliquot of labeled virus was introduced into the inlet reservoir, closest to the largest gate (Gate 1 in Fig. 1), using micropipette. Running buffer was added in the outlet reservoir to eliminate the pressure driven flow. Two platinum wire electrodes (0.25 mm diameter, 99.997% purity, Alfa Aesar, Ward Hill, MA, USA) were placed, one in each reservoir, with both connected to a high voltage power supply (HVS 448 High Voltage Sequencers, LabSmith Inc., Livermore, CA, USA). The sample solution was introduced into the microchannel through the inlet reservoir and was allowed to flow until several channel volumes had passed, assuring viral particles are evenly distributed throughout the whole channel. The electrical potential was applied across the microchannel (V_{app}), ranging from 0-700 V, while the behavior of viral particles was examined throughout the whole channel. The applied voltage time varied from a few seconds up to one minute for multiple experiments and sample preparations.

Separation and Data Collection

The SVHR behavior in the DEP device was monitored using an Olympus IX70 inverted microscope in epi-fluorescence configuration. Light was detected with a QICAM CCD camera (Q Imaging, Surrey, British Columbia, Canada) and recorded using a commercial program (Stream Pix V program, NorPix, Montreal, Quebec, Canada). Further image processing were performed using Image J (U. S. National Institutes of Health, Bethesda, Maryland, USA).

Safety Consideration

SVHR is a biosafety level (BSL) II agent. All procedures were performed in BSL II approved space.

Results

Improvement of Microchannel Design

The electric potential distribution within a channel was modeled with finite-element multiphysics software. Two primary concerns were the improvement of g-iDEP resolving capabilities and extension of capture range to smaller analytes including submicron bioparticles. The existing V1 microchannel geometry proved well-suited for capturing relatively large-scale bioanalytes including a variety of cell types.[49-51] However, insufficient DEP force was generated to capture smaller analytes. Unpublished work demonstrated an inability of V1 microchannel to capture norovirus capsid and proteins (data not shown).

Modeling confirmed that the original V1 microchannel geometry created values of e_c were insufficient for the capture of small, submicron analytes. Even relatively large species were only captured near the final sets of gates,[48-51] where the highest maxima of e_c occurred. Furthermore, the magnitudes of local maxima in e_c increased exponentially at gates along the channel (Fig. 2-A). This led to minimal variation in e_c along most of the channel length, and thus reduced capacity for resolving different analytes.

In an effort to iteratively improve the capabilities and applicability of g-iDEP microchannel, a new microchannel (designated V2) was designed for use with small bioparticles such as viruses and proteins. It features initial and final gate pitches of 30 and 3 μm, respectively.

To enable future attempts to resolve similar analytes, V2 design also features more incremental stair-steps in pitch between sets of gates (Fig. 2-B and 2-C). This offers the potential to improve resolution of analytes by creating a series of more finely tuned and graduated dielectrophoretic traps. Each trap is then capable of distinguishing smaller gradations in particle characteristics ($\Delta[\mu_{EK}/\mu_{DEP}]$). To design these step-sizes, modeled values of e_c were related to gate pitch (p) by a power function (Fig. 2-B). The specific values of e_c are related to additional inputs, including the applied voltage and the specific

channel geometry. Using this data, a set of progressively decreasing p values was calculated, that would yield a linear increase in the maxima of e_c across a channel.

Models of the new channel geometry confirmed a more regulated, step-wise increase in $\nabla E^2/E$ across the centreline of the channel (Fig. 2-C).

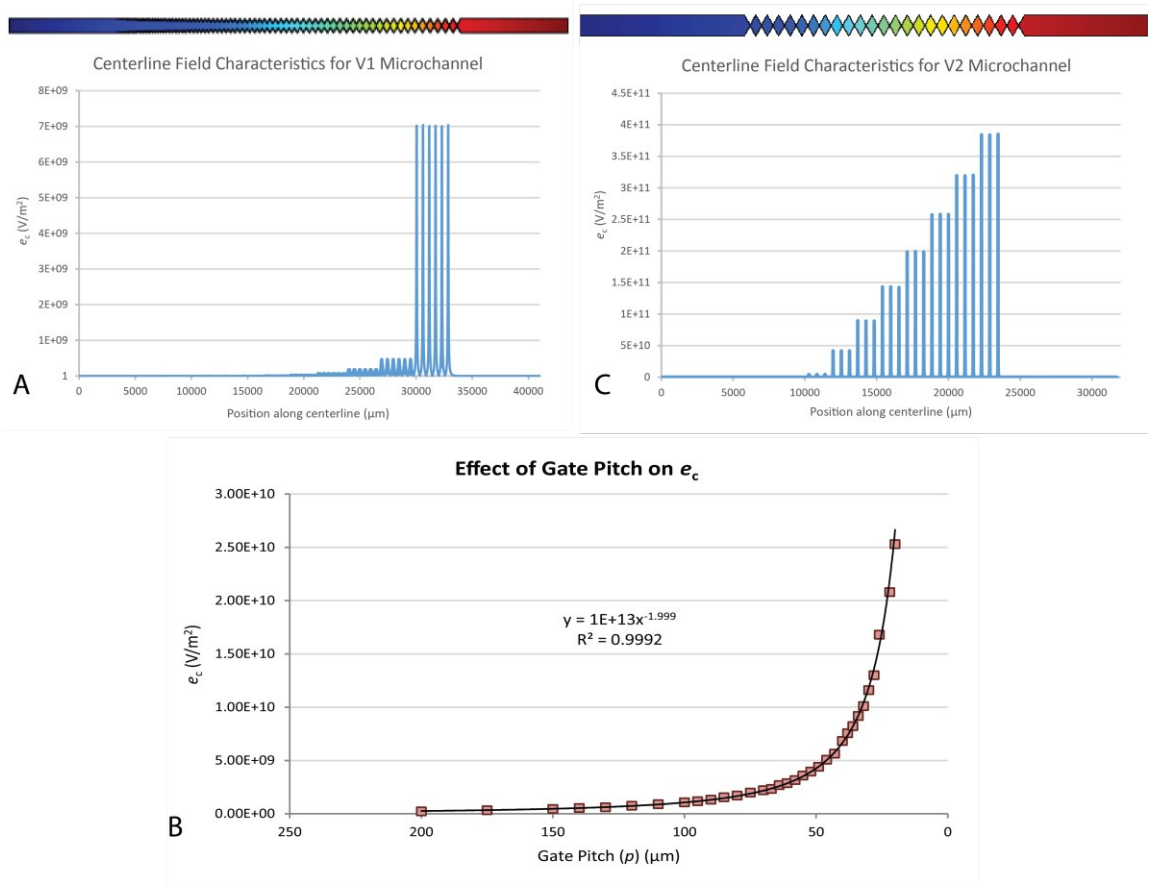

Figure 2. Comparison of microchannel designs between V1 and V2. The channel inlet and large *p* values are oriented to the left, while the outlet and small *p* values are oriented to the right. (A) Centerline values of $\nabla E^2/E$ (or e_c) modeled for the V1 microchannel. Specific values for $\nabla E^2/E$ depend upon channel geometry and the applied potential (500 V for this model). Each set of gates consists of 6 geometrically equivalent gates, all with equal pitch. (B) Chart showing centerline maxima in e_c for a hypothetical sawtooth microchannel. Values for e_c are represented as a function of *p* (pitch, or distance between tooth tips at gates). The increase in e_c with respect to *p* can be represented as a power function. (C) Centerline values of $\nabla E^2/E$ modeled for a V2 microchannel. A progression of values for *p* was calculated to yield a linear step-wise increase in the local maxima of $\nabla E^2/E$ between gate sets. Each set consists of three geometrically equivalent gates, all with equal *p*.

Characterization of Sindbis Virus

The target virus, SVHR, was characterized for size and morphology, before and after labeling treatment (Fig. 3). DLS was performed to define the size distribution of the unlabeled particles. A large majority of the SVHR particles are shown to have a radius of about 46 nm, with some particles a bit smaller or larger, which might be the fragments of broken viruses or the aggregated viral particles caused by these fragments (Fig. 3-A). After labeling, SVHR had a narrower distribution of size (Fig. 3-B), but centered at a higher radius of 56 nm. These values reasonably agree with the theoretical radius of SVHR (r = 34 nm[62]) considering that the size measured from DLS is the equivalent hydrodynamic radius, which is usually larger than the actual physical radius. The heat maps of the light scattering intensity corresponding to the SVHR sample before and after labeling were also examined (Fig. 3-C and 3-D). The scattered light intensity is mainly from viral particles with restricted size range throughout the measuring period. The narrow distribution and consistent results are indications of no significant aggregation of virus, which shows that the SVHR sample is in a highly monodispersed state.

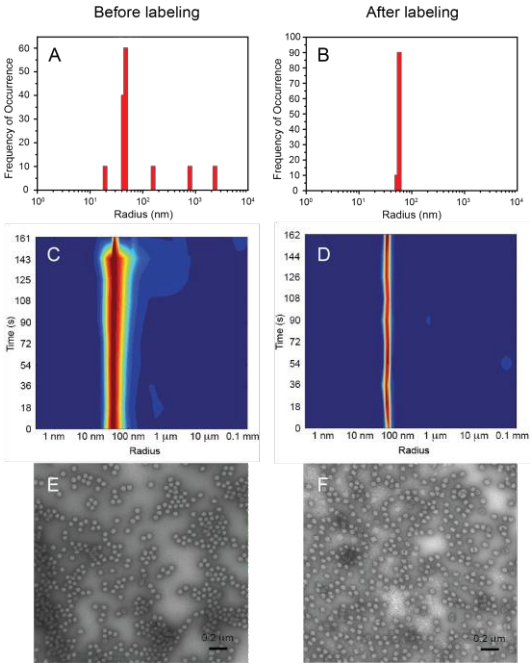

Figure 3. Characterization of SVHR viral particles by DLS and TEM before and after labeling. Size analysis by DLS measurement: histogram of size distribution (A, before and B, after) and heat maps (C, before and D, after). Histogram data indicates viral particles average 46.3 nm before labeling and 56.4 nm after. Heat maps provide temporal information for ten separate 20 s measurement that can detect polydispersity (blue for lowest intensity and red for highest). Data indicate a monodisperse population and a shift to larger size for labeled population. Visual inspection before (E) and after (F) labeling was recorded via TEM. The shape of the virions vary little, presenting a semispherical outline for both populations. Size estimation from 100 particle features from each figure confirms uniformity, with the labeled virus slightly larger—in agreement with the DLS results.

TABLE 1. Size of Sindbis virus determined by DLS and TEM

Sample	DLS (r_{virus})	TEM (r_{virus})
Original Virus	46.3 ± 2.1 nm	34.6 ± 2.2 nm
Labeled Virus	56.4 ± 1.7 nm	34.8 ± 2.2 nm

Transmission electron microscopy also produced unambiguous results. Individual light grey circular structures, surrounded by diffuse darker rings, were apparent throughout all images (Fig. 3-E and 3-F). Few or no broken circles or joined, irregular features, consistent with damage or aggregation were noted. There were no significant morphological or size changes between the two samples and the diameter from 100 circular structures (for each sample) was 69.2 ± 4.4 nm (unlabeled) and 69.6 ± 4.3 nm (labeled). The result shows a good agreement with the literature report.[62]

Dielectrophoretic Capture of Sindbis Virus

The labeled SVHR was injected into the g-iDEP devices. The gates with a gap width of 3.3 μm demonstrated consistent visible capture for all trials (without obvious errors such as bubbles or clogging). The 20th gate, which is the middle gate of the set of three, was chosen for detailed quantitative assessment (Fig. 4) since it was not the last set of gates and capture occurred at low voltage. These studies were captured with fluorescence imaging and combined light-field and dark-field illuminations. Before the voltage was applied, the SVHR sample solution was evenly distributed throughout the whole channel and no obvious fluorescence was seen in the channel (Fig. 4-A). Upon application of the voltage, viral particles began moving toward the outlet reservoir and simultaneously began to trap and thus accumulate at the outlet side of the gate. Over the application of V_{app} for 15 s, clear increase in fluorescence intensity can be observed within the capturing zone (Fig. 4-B). Considering that the dominant movement in the microchannel is the electrokinetic flow towards the outlet (blue arrows in Fig. 4-B), the capture at the outlet side of the gate is consistent with the positive dielectrophoresis (white arrows in Fig. 4-B). No accumulation is observed at the inlet or left side of the gate. Electrokinetic and dielectrophoretic forces are additive in this zone and the particles are accelerated. After removing the voltage, the viral particles released and are observed to diffuse to the surrounding solution (Fig. 4-C).

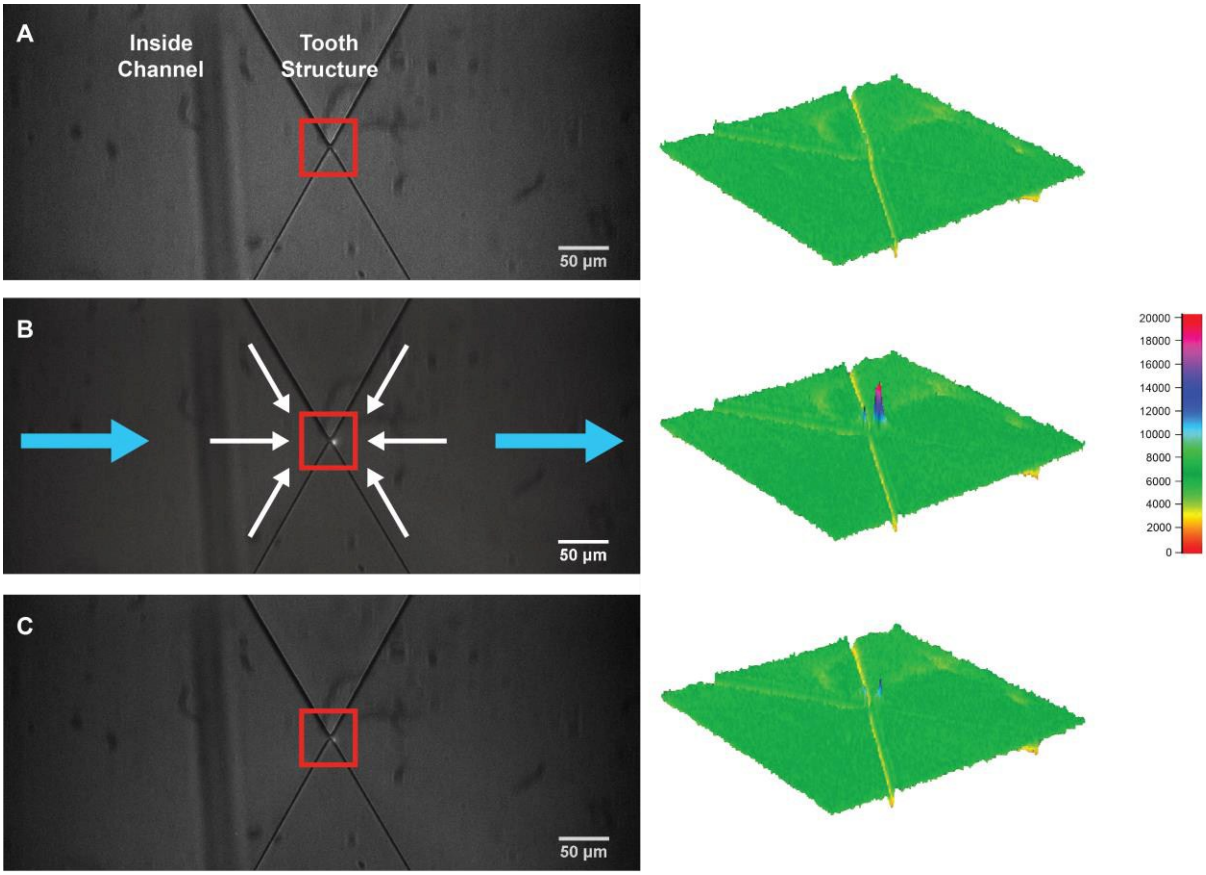

Figure 4. Images of virus accumulation and release at gate 20. (A) Evenly distribution of viral particles. No obvious fluorescence is detectable near the constriction prior to application of the voltage. (B) After 15 s with 300 V applied on the whole channel, there is clear accumulation of the fluorescent particles on the outlet side (right side) of the gate, represented as a constricted peak in the capturing zone in the corresponding fluorescent profile. Blue arrows indicate the direction of electrokinetic forces, while the white arrows are the directions of *p*DEP force. (C) Captured particles diffused away upon the removal of the voltage. Most fluorescence disappears at the region of capture. The surface plots on the right are the fluorescence intensity profiles of the area in the corresponding red boxes in the images.

The applied voltage was varied from 100 V to 600 V with 100 V increments (Fig. 5). Integrated fluorescence intensity (FI) was measured at the capture region for each value. FI increased rapidly with time for values of above 200 V (Fig. 5-A). Intensity measurements were taken at time point 20 s, when V_{app} had been on for 15 s (Fig. 5-B), where FI increases dramatically with the increased V_{app}. All FI measurements were acquired after applying V_{app} for the same period of time (15 s), indicating higher values of V_{app} result in faster accumulation of viral particles. The virions are transported and accumulated faster since local velocity is $\nu_{ep} = \mu_{ep} E$ and E is a direct function of V_{app}.

The behavior of virus in the g-iDEP device indicated that there was a potential transition from noncapturing to capturing when moving to higher V_{app}. To examine this transition, V_{app} was varied between 0 and 100 V at a smaller increment of 10 V and the FI was investigated (Fig. 5-C). Combining with the results obtained at higher V_{app} (>100 V) data consistently generates a pattern of three stages: no obvious capture at low V_{app} (< ~50-70 V), steadily rising FI with increasing voltage (~70 to 200 V) where significant capturing occurs, and stable FI with increasing voltage (greater than 200 V).

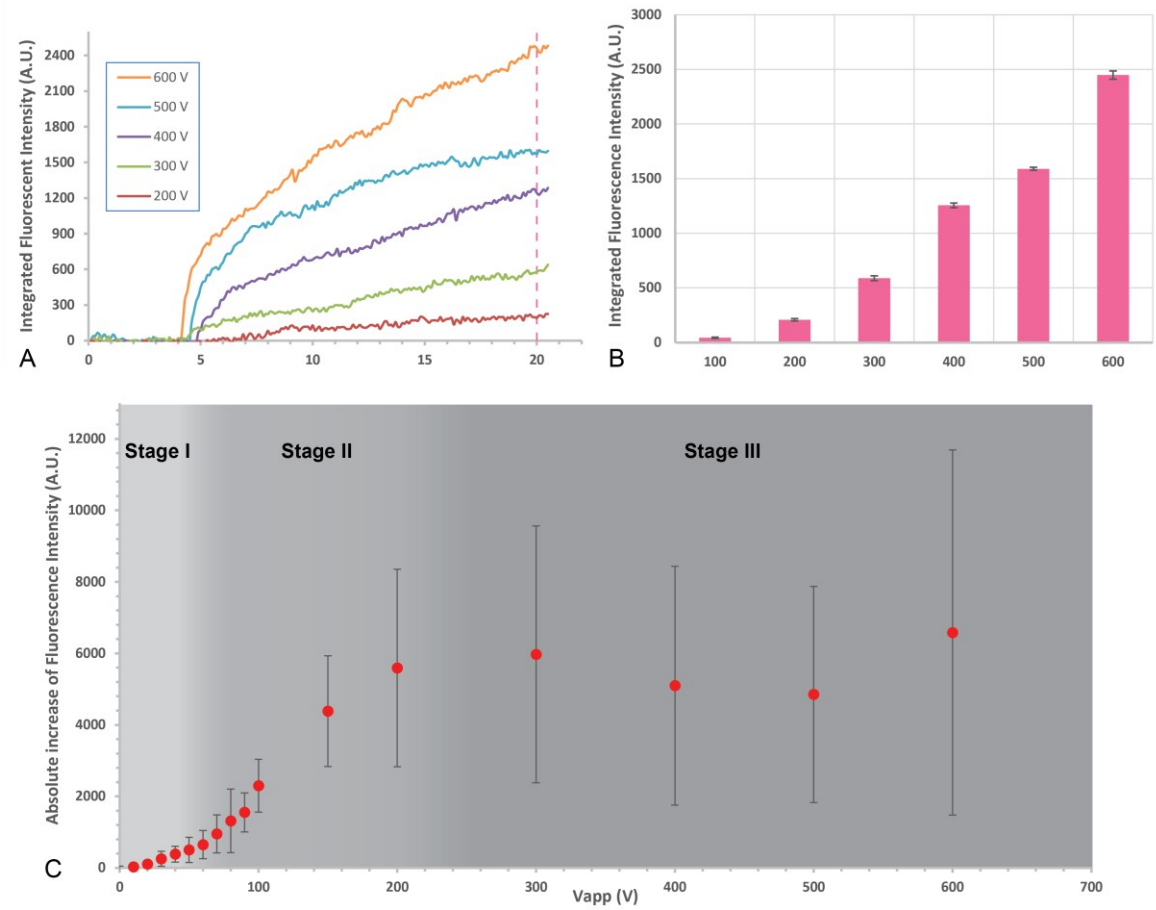

Figure 5. Data analysis of SVHR behavior at gate 20 (3.3 µm gap distance) with different V_{app}. The concentration of SVHR is 1.5 x 10^{11} pfu/mL. (A) Real-time monitoring of integrated fluorescence intensity (FI) increase versus time with V_{app} from 100 V to 600 V. (B) The integrated FI of the capturing zone with V_{app} being on for the duration of 15 s, replot from the data at 20 s time point in A (indicated by the dashed line in A) at each V_{app}. Error bars are based on the ten data points for ± 0.5 s. (C) By repeating the experiments with independent preparation of SVHR samples and each in a separated device, lower applied voltages between 0 V and 100 V were tested for more comprehensive understanding of the change of FI versus V_{app}. The virus behavior shows in a stage-wise way with little or no capture at low voltages (stage I), rapid increase with increased V_{app} (stage II) and leveling off during plateau (stage III). Error bars are the standard deviation (n=3).

By repeating the experiments with independent preparation of SVHR samples in separated devices, the results demonstrated a good reproducibility of virus manipulation. Corresponding data analysis by comparing the fluorescent intensity change at the capturing zone also revealed an intensity increase of SVHR by two to six times within 15 s (original data not shown).

Discussion

Device Design

Generally, the sawtooth design of the g-iDEP device is aimed at selective capture of a variety of bioparticles at different locations in the channel. The isolated/purified biological samples are envisioned to be used for direct identification or further clinical testing and characterization. Simulations for the original V1 design indicate that the characteristic factor, e_c, varied with gate number as a power function (Fig. 2-C), where only the last few gates gave high enough e_c to capture anything of note. Based on experimental results, this e_c is in the range of 10^9 V/m^2 for bioparticles in micrometer range, with *Staphylococcus epidermidis* at between 4.6 and 9.2 $\times 10^9$ V/m^2 and *E. coli* within around 6.8 to 13.6 $\times 10^9$ V/m^2, and red blood cell (RBC) are estimated to be at around 2.8 $\times 10^9$ V/m^2.[49,51,52]

The requirements of the new design were examined. In the same experimental environment when solution permittivity (ε), conductivity (c), viscosity (η) remain the same, μ_{EK} only varies with the zeta potential of the particle while $\mu_{DEP} = \frac{\varepsilon r_p^2 Re\{f_{cm}\}}{3\eta}$ is strongly influenced by the radius (r_p) and less so by the Clausius-Mossotti factor ($Re\{f_{cm}\}$).[63] However, the zeta potential of bioparticles is fairly consistent and generally does not range by more than 100 mV while Clausius-Mossotti factor is bounded by the limits ($-\frac{1}{2}$ to 1) shown by its definition ($Re\{f_{cm}\} = Re\{\frac{\varepsilon_p^* - \varepsilon_m^*}{\varepsilon_p^* + 2\varepsilon_m^*}\}$)[64](although asymmetric particle can exceed this somewhat). In this way, the ratio of $\frac{\mu_{EK}}{\mu_{DEP}}$ can be simplified to be proportional to $\frac{1}{r_p^2}$. This means that smaller particles increase the ratio of $\frac{\mu_{EK}}{\mu_{DEP}}$ and that higher e_c values would be necessary for smaller particle trapping.

Previous studies show that the threshold e_c values for different bioparticles are relatively close. For example, the threshold e_c values for different *Staphylococcus epidermidis* strains differ by ~5 $\times 10^9$ V/m^2.[52] Similar phenomenon has also been proven with different strains of *E. coli*.[51] By noting that the e_c value is related to gate pitch (p), smaller intervals were chosen to minimize differences in e_c values between adjacent sets of gate. In this way, smaller difference of e_c values would help trap different particles which have similar properties and result in close $\frac{\mu_{EK}}{\mu_{DEP}}$ values.

With respect to submicron particles, the magnitude of e_c needs to be increased. To separate similar particles, the increment of e_c between gates was linearized (along with reduced differences). These features provide the potential to capture and separate smaller targets including submicron bioparticles, such as viruses (mainly 20 – 300 nm in diameter[65]) and

proteins (1 – 100 nm[66]). Based on this modified design, simulations indicated a high enough e_c for potential smaller targets, enhanced by two orders of magnitude compared with the highest e_c produced in V1 microchannel (Fig. 2-B). The smallest pitch was set to be 3 μm to be within the photomask fabrication limitation. With 500 V applied arcoss the channel, the e_c value on the centerline of the smallest gate (3 μm) in V2 microchannel can be as high as 3.84×10^{11} V/m^2, some 50 times higher than the highest e_c value (7.02×10^{9} V/m^2) on the centerline that can be generated in V1 channel under the same condition.

This newly improved design (V2) has been used in all experiments reported in this work and demonstrated its improved ability and verified the simulation. The successful capture of SVHR also demonstrates this V2 channel does have the ability of capturing submicron particles. No capture of other submicron particles (norovirus capsid, various proteins) in V1 channel was observed (data not shown). This new design shifts the capture of smaller particles to second smallest set of gates in the new design.

Behavior of Sindbis Virus in g-iDEP Devices

Using the labeled inactivated SVHR with the V2 microchannel device, capture and accumulation were observed and analysed. The behavior of SVHR is consistent with *p*DEP in our channel geometry and applied field direction. Positive DEP behavior has been observed with other viruses noted above.[31,39,42,44] When the potential is removed, the FI dissipates quickly, indicating that the trapped virions were freely diffusing even after capture and show reversible capture behavior. Considering e_c is related to electric field (E) and pitch size (p), higher e_c can be generated with increased applied voltage while pitch sizes are fixed in the channel. The result indicates that at longer time and at higher V_{app} facilitated increased accumulation. By tuning V_{app} from zero to 600 V, the behavior of virus in the device indicates there is a transition from zero capture (flowing through) to definitive capture (Fig. 5). This trend can generally be described by a sigmoidal shape and we term the three stages I (< ~50-70 V), II (~70 to 200 V) and III (greater than 200 V) for discussion purposes.

Within stage I, the electrokinetic force dominates and e_c is too small for capture. All the virions flow through the channel from inlet to outlet with electrokinetic flow. Virions may be influenced by dielectrophoretic forces and stream (lateral offset) through the gate areas, although neither of these actions can be explicitly observed. They are inferred by the actions at slightly higher voltages.

Within stage II, with V_{app} above a certain threshold (around 70 V), e_c is large enough for capture. All virions that enter the accumulation zone are retained and the transport of virions increases with higher local electric field (E), which is related to V_{app}. The integrated FI changes approximate a linear relationship from 80 V to 200 V of V_{app}, consistent with the electrokinetic transport and full capture mechanisms.

Within in Stage III (> 200 V), FI reaches a relatively stable, but noisy level. There are two possible mechanisms for this plateau. One is that the FI in the region of interest (ROI)

reaches the saturation of the CCD camera. Even though more viral particles being transported and captured in ROI at higher V_{app}, the CCD camera cannot detect the correspondingly increased FI, showing as a plateau in Fig. 5-C. The second possibility is depletion. At each gate, most virions being captured have been transported from the local solution on the left of the gate. If the gate prior to the collection gate is also capturing virions (true at higher V_{app}), then the volume where the virions could be collected is depleted and no further capture is possible. This is not true for temporal collections, as the volume available for depletion reaches into the sample reservoir. Corresponding data analysis also demonstrates that the concentration of SVHR was increased by about two to six times within 15 s with this limitation by saturation.

It is also interesting to notice that there is a soft transition from the non-capture to capture instead of a distinct change (Fig. 5-C). This phenomenon is probably due to that the dielectrophoresis is not consistent on the vertical direction, which is much higher near the insulator wall than that in the center region on the same vertical location. In this way, there is a possibility some virions were retained locally if they are extremely close to the sawtooth tips (at lower V_{app}) where the dielectrophoresis is much stronger. Accumulation was observed to begin near the sawtooth tip and built up gradually to the center of the channel. This phenomenon also suggest specific issues to address in further improved designs for sharper and more distinct transition from no capture to capture.

Structural Analysis on DEP behavior of SVHR

At current stage, SVHR must be labeled for real time monitoring and quantification. The structure and size distribution remained relatively consistent before and after labeling. Slightly more homogeneous size distribution is observed after labeling (Fig. 3-C and 3-D). Virus particles tend to form aggregations that settle, removing a sub-population. The attached dye moiety may improve stability though altered hydrophobicity and inter-particle interactions, preventing degradation or aggregation.

The structure of SVHR has been well studied. From outer shell to inner core, there are three components: a lipid bilayer embedded with glycoproteins E1 and E2 (envelope), a protein layer (capsid) and the RNA genome core. Both envelope and capsid make up the icosahedral structure, which can be reasonably approximated as two concentric spherical shells.[67] This spherical shape simplifies the estimation of dielectrophoretic forces (allowing an assumption of a simple ~70 nm[55] sphere).

The electrokinetic behavior of SVHR is consistent with *p*-DEP. For the Clausius-Mossotti relationship to hold, conductivity of the particle must be larger than the medium (2.12 mS/cm). Among the three main components of SVHR, lipid bilayer in the envelope has a low conductivity ($< 10^{-8}$ S/m) and contributes little to the overall conductivity. However, the glycoproteins in the envelope and capsid proteins may significantly influence the overall dielectric properties of SVHR. The glycoproteins, E1 and E2 (embedded in the lipid bilayer) and the capsid are anchored together through interaction between the glycoprotein E2 endodomain

with capsid proteins.[67] The charged residues in the proteins as well as the interaction between proteins from outer shell to inner core would increase the conductivity of the whole viral particle. Similar impact of structural proteins on the electric properties of other viruses has also been demonstrated in previous research.[68] The conformational structure of virus changes accordingly with varying experimental conditions.[67] Noting all these factors, the core structure of the virus particle still has a relatively low conductivity compared to the buffer. Instead, the surface conductance resulting from the electric double layer is the most likely contributor to the demonstrated conductivity.

At pH=7.2, the SVHR is negatively charged (pI of 4.2).[69] The corresponding electrophoretic movement is towards the outlet reservoir, which is in the same direction with the bulk electroosmosis. During labeling, the dye molecule replaces the primary amine groups on the side chain of lysine. At pH=7.2, lysine is positively charged while the dye molecule has a net charge of zero. Labeled SVHR is more negatively charged, which would increase the electrokinetic velocity as well as increasing the dielectrophoresis by increasing the corresponding surface conductivity. This is still largely speculative and dielectric properties of virus are in need of more experimental investigations and theoretical modeling.

Application of the Method for Manipulating Submicron Bioparticles.

The capture and accumulation of SVHR in this work demonstrates the capabilities of using the V2 microchannel for small analytes, especially submicron bioparticles, in this case viral particles. According to the results, the V2 microchannel device shows virus capture and release ability. More than that, the voltage-dependent capturing behavior was studied and a threshold voltage value was estimated. These results indicate a potential for clinical and diagnostic applications, where bioparticles such as cells, virus, and proteins play crucial roles. Since the dielectrophoretic property varies with the composition, shape, size and charge of the target analyte, it is expected that different kinds of bioparticles would have unique dielectrophoretic behavior resulting from the structural variations. Currently, this device is still at its preliminary developing stage and operates in an analytical mode, simply capturing and concentrating the viral particles. Further improvement by integrating orthogonal side channels and valves onto the main channel will realize the control on the delivery of the concentrated sample. With valves, these side channels can be held electric silent during capture and be activated to transport the concentrated virus sample to further analysis either on-chip or off-chip. Instead of using conventional time-consuming methods, this rapid response technique would benefit clinical diagnostics/detection in the future.

Conclusions

With the improved microchannel design for the g-iDEP device aiming at submicron particles, the Sindbis virus was successfully captured under DC fields with easily achievable low potentials.

Previous work demonstrates the viability of using V1 microchannel for capturing particles, such as polystyrene particles, protein amyloid fibrils, red blood cells and bacteria, though most

capture and concentration of particles were observed at last two sets of gates while all larger gates showed little evidence of capture. This newly improved design overcomes this by creating a higher characteristic e_c value increasing linearly throughout the channel, which realizes the capture for small particles. Further investigation demonstrated the reproducibility of capture and concentration Sindbis virus with the new microchannel design. These results bear important meanings for the future of virus detection and even the promising prospects of clinical analysis in fields such as point-of-care (POC) application.

Acknowledgement

This work was supported by National Institutes of Health grants 1R03AI094193-01, 1R03AI099740-01, and R03AI111361-01 and in part by National Science Foundation (NSF) Award No. 1120997, NSF STC BioXFEL Center Award No. 1231306

The authors have declared no conflict of interest.

References

1. K. Kamimura, T. Suda, G. Zhang and D. Liu, *Pharmaceut Medicine*, 2011, **25**, 293-306.
2. E. Galanis, *Nature*, 2011, **477**, 40-41.
3. C. J. Breitbach, J. Burke, D. Jonker, J. Stephenson, A. R. Haas, L. Q. M. Chow, J. Nieva, T. H. Hwang, A. Moon, R. Patt, A. Pelusio, F. Le Boeuf, J. Burns, L. Evgin, N. De Silva, S. Cvancic, T. Robertson, J. E. Je, Y. S. Lee, K. Parato, J. S. Diallo, A. Fenster, M. Daneshmand, J. C. Bell and D. H. Kirn, *Nature*, 2011, **477**, 99-U102.
4. T. L. A. Nguyen, V. F. Tumilasci, D. Singhroy, M. Arguello and J. Hiscott, *Cell Microbiol.*, 2009, **11**, 889-897.
5. B. N. Fields, D. M. Knipe and P. M. Howley, *Fields virology*, Wolters Kluwer Health/Lippincott Williams & Wilkins, Philadelphia, 2013.
6. S. J. Flint, *Principles of virology: molecular biology, pathogenesis, and control of animal viruses*, ASM Press, Washington, D.C, 2004.
7. F. D'Herelle and G. H. Smith, *The bacteriophage and its behavior / by F. d'Herelle translated by George H. Smith*, The Williams & Wilkins Company, Baltimore, Md. :, 1926.
8. K. Maramorosch and H. Koprowski, *Journal*, 1967, 313-336.
9. K. Habel, N. P. Salzman and S. Baron, *Fundamental techniques in virology*, Academic Press, New York, 1969.
10. L. J. REED and H. MUENCH, *American Journal of Epidemiology*, 1938, **27**, 493-497.
11. I. D. Odell and D. Cook, *J Invest Dermatol*, 2013, **133**, e4.
12. J.-M. Fritschy and W. Härtig, in *eLS*, John Wiley & Sons, Ltd, 2001, DOI: 10.1038/npg.els.0001174.
13. E. T. Lennette, S. Karpatkin and J. A. Levy, *Journal of clinical microbiology*, 1987, **25**, 199-202.
14. A. Voller, D. E. Bidwell and A. Bartlett, *Lab Res Methods Biol Med*, 1982, **5**, 59-81.
15. T. G. Ksiazek, C. P. West, P. E. Rollin, P. B. Jahrling and C. J. Peters, *Journal of Infectious Diseases*, 1999, **179**, S192-S198.
16. M. L. Edwards and J. I. Cooper, *J Virol Methods*, 1985, **11**, 309-319.
17. J. Renart, J. Reiser and G. R. Stark, *Proc Natl Acad Sci U S A*, 1979, **76**, 3116-3120.
18. S. R. Pereira, C. E. Travassos, A. Huguenim, A. C. Guimaraes, A. G. Silva and M. A. Guimaraes, *Brazilian Journal of Medical and Biological Research*, 1998, **31**, 671-674.
19. S. Specter, R. L. Hodinka and S. A. Young, *Clinical virology manual*, ASM Press, Washington, DC, 2000.
20. D. C. Baulcombe, S. Chapman and S. Santa Cruz, *The Plant journal : for cell and molecular biology*, 1995, **7**, 1045-1053.
21. I. M. Mackay, K. E. Arden and A. Nitsche, *Nucleic Acids Res.*, 2002, **30**, 1292-1305.
22. F. Cobo, *The open virology journal*, 2012, **6**, 104-114.
23. C. S. Goldsmith and S. E. Miller, *Clinical microbiology reviews*, 2009, **22**, 552-563.
24. M. Adrian, J. Dubochet, J. Lepault and A. W. McDowall, *Nature*, 1984, **308**, 32-36.
25. W. Zhang, S. Mukhopadhyay, S. V. Pletnev, T. S. Baker, R. J. Kuhn and M. G. Rossmann, *Journal of Virology*, 2002, **76**, 11645-11658.
26. J. E. Lawrence and G. F. Steward, *Manual of Aquatic Viral Ecology*, 2010, DOI: 10.4319/mave.2010.978-0-9845591-0-7.166, 166-181.
27. C. Charcosset, *Biotechnology Advances*, 2006, **24**, 482-492.
28. T. A. Grein, Z. Kovacs, M. Ebrahimi, R. Michalsky and P. Czermak, *Chemie Ingenieur Technik*, 2013, **85**, 1183-1192.
29. B. Kalbfuss, Y. Genzel, M. Wolff, A. Zimmermann, R. Morenweiser and U. Reichl, *Biotechnology and bioengineering*, 2007, **97**, 73-85.
30. B. Kalbfuss, D. Flockerzi, A. Seidel-Morgenstern and U. Reichl, *Journal of Chromatography B-Analytical Technologies in the Biomedical and Life Sciences*, 2008, **873**, 102-112.
31. I. Ermolina, J. Milner and H. Morgan, *Electrophoresis*, 2006, **27**, 3939-3948.
32. F. Grom, J. Kentsch, T. Muller, T. Schnelle and M. Stelzle, *Electrophoresis*, 2006, **27**, 1386-1393.
33. B. H. Lapizco-Encinas and M. Rito-Palomares, *Electrophoresis*, 2007, **28**, 4521-4538.
34. C. Zhang, K. Khoshmanesh, A. Mitchell and K. Kalantar-zadeh, *Analytical and Bioanalytical Chemistry*, 2010, **396**, 401-420.
35. T. Muller, S. Fiedler, T. Schnelle, K. Ludwig, H. Jung and G. Fuhr, *Biotechnol. Tech.*, 1996, **10**, 221-226.
36. T. Schnelle, T. Muller, S. Fiedler, S. G. Shirley, K. Ludwig, A. Herrmann, G. Fuhr, B. Wagner and U. Zimmermann, *Naturwissenschaften*, 1996, **83**, 172-176.
37. N. G. Green and H. Morgan, *Journal of Physics D-Applied Physics*, 1997, **30**, 2626-2633.
38. N. G. Green, H. Morgan and J. J. Milner, *J. Biochem. Biophys. Methods*, 1997, **35**, 89-102.
39. H. Morgan, M. P. Hughes and N. G. Green, *Biophysical Journal*, 1999, **77**, 516-525.
40. M. P. Hughes, H. Morgan, F. J. Rixon, J. P. H. Burt and R. Pethig, *Biochimica Et Biophysica Acta-General Subjects*, 1998, **1425**, 119-126.
41. M. P. Hughes, H. Morgan and F. J. Rixon, *Biochimica Et Biophysica Acta-General Subjects*, 2002, **1571**, 1-8.
42. M. P. Hughes, H. Morgan and F. J. Rixon, *Eur. Biophys. J. Biophys. Lett.*, 2001, **30**, 268-272.
43. K. F. Hoettges, M. B. McDonnell and M. P. Hughes, *Electrophoresis*, 2014, **35**, 467-473.
44. B. H. Lapizco-Encinas, B. A. Simmons, E. B. Cummings and Y. Fintschenko, presented in part at the Procedding of the 7th International Conference on Micro Total Analysis Systems, Squaw Valley CA, USA, 2003.

45. B. H. Lapizco-Encinas, R. V. Davalos, B. A. Simmons, E. B. Cummings and Y. Fintschenko, *Journal of Microbiological Methods*, 2005, **62**, 317-326.
46. T. Masuda, H. Maruyama, A. Honda and F. Arai, *PloS one*, 2014, **9**, e94083.
47. M. D. Pysher and M. A. Hayes, *Analytical Chemistry*, 2007, **79**, 4552-4557.
48. S. J. R. Staton, K. P. Chen, T. J. Taylor, J. R. Pacheco and M. A. Hayes, *Electrophoresis*, 2010, **31**, 3634-3641.
49. P. V. Jones, S. J. Staton and M. A. Hayes, *Anal Bioanal Chem*, 2011, **401**, 2103-2111.
50. S. J. R. Staton, P. V. Jones, G. Ku, S. D. Gilman, I. Kheterpal and M. A. Hayes, *Analyst*, 2012, **137**, 3227-3229.
51. P. V. Jones, A. F. DeMichele, L. Kemp and M. A. Hayes, *Analytical and Bioanalytical Chemistry*, 2014, **406**, 183-192.
52. P. V. Jones, S. Huey, P. Davis, R. McLemore, A. McLaren and M. A. Hayes, *Analyst*, 2015, **140**, 5152-5161.
53. A. Gencoglu, D. Olney, A. LaLonde, K. S. Koppula and B. H. Lapizco-Encinas, *Electrophoresis*, 2014, **35**, 362-373.
54. J. O. Lundstrom and M. Pfeffer, *Vector borne and zoonotic diseases (Larchmont, N.Y.)*, 2010, **10**, 889-907.
55. S. D. Fuller, *Cell*, 1987, **48**, 923-934.
56. A. M. Paredes, D. T. Brown, R. Rothnagel, W. Chiu, R. J. Schoepp, R. E. Johnston and B. V. Prasad, *Proc Natl Acad Sci U S A*, 1993, **90**, 9095-9099.
57. A. M. Paredes, H. Heidner, P. Thuman-Commike, B. V. Prasad, R. E. Johnston and W. Chiu, *J Virol*, 1998, **72**, 1534-1541.
58. R. Hernandez, C. Sinodis and D. T. Brown, *Current protocols in microbiology*, 2005, **Chapter 15**, Unit 15B.11.
59. M. A. K. Markwell, S. M. Haas, L. L. Bieber and N. E. Tolbert, *Anal. Biochem.*, 1978, **87**, 206-210.
60. C. Mack, *Fundamental Principles of Optical Lithography: The Science of Microfabrication*, Wiley, 2008.
61. P. V. Jones and M. A. Hayes, *Electrophoresis*, 2015, **36**, 1098-1106.
62. D. T. Brown, M. R. Waite and E. R. Pfefferkorn, *J Virol*, 1972, **10**, 524-536.
63. N. G. Weiss, P. V. Jones, P. Mahanti, K. P. Chen, T. J. Taylor and M. A. Hayes, *Electrophoresis*, 2011, **32**, 2292-2297.
64. I. Ermolina and H. Morgan, *J. Colloid Interface Sci.*, 2005, **285**, 419-428.
65. A. M. Q. King, E. Lefkowitz, M. J. Adams and E. B. Carstens, in *Virus Taxonomy*, eds. A. M. Q. King, M. J. Adams, E. B. Carstens and E. J. Lefkowitz, Elsevier, San Diego, 2012, DOI: http://dx.doi.org/10.1016/B978-0-12-384684-6.00114-2, pp. 1-20.
66. H. P. Erickson, *Biol. Proced. Online*, 2009, **11**, 32-51.
67. L. He, A. Piper, F. Meilleur, R. Hernandez, W. T. Heller and D. T. Brown, *J Virol*, 2012, **86**, 1982-1987.
68. R. I. MacCuspie, N. Nuraje, S. Y. Lee, A. Runge and H. Matsui, *J Am Chem Soc*, 2008, **130**, 887-891.
69. J. M. Dalrymple, S. Schlesinger and P. K. Russell, *Virology*, 1976, **69**, 93-103.